Reconstruction of radial thermal conductivity depth profile in case hardened steel rods

Ricardo Celorrio,[1] Arantza Mendioroz,[2] Estibaliz Apiñaniz,[2] Agustín Salazar,[2,a)] Chinhua Wang,[3] and Andreas Mandelis[4]
[1]*Departamento de Matemática Aplicada, EUITIZ, Universidad de Zaragoza, Campus Río Ebro, Edificio Torres Quevedo, 50018 Zaragoza, Spain*
[2]*Departamento de Física Aplicada I, Escuela Técnica Superior de Ingeniería, Universidad del País Vasco, Alameda Urquijo s/n, 48013 Bilbao, Spain*
[3]*Institute of Modern Optical Technologies, Soochow University, Suzhou, Jiangsu 215006, People's Republic of China*
[4]*Department of Mechanical and Industrial Engineering, Center for Advanced Diffusion-Wave Technologies, University of Toronto, Toronto, Ontario, M5S 3G8, Canada*

(Received 29 December 2008; accepted 21 February 2009; published online 20 April 2009)

In this work the surface thermal-wave field (ac temperature) of a solid cylinder illuminated by a modulated light beam is calculated first in two cases: a multilayered cylinder and a cylinder the radial thermal conductivity of which varies continuously. It is demonstrated numerically that, using a few layers of different thicknesses, the surface thermal-wave field of a cylindrical sample with continuously varying radial thermal conductivity can be calculated with high accuracy. Next, an inverse procedure based on the multilayered model is used to reconstruct the radial thermal conductivity profile of hardened C1018 steel rods, the surface temperature of which was measured by photothermal radiometry. The reconstructed thermal conductivity depth profile has a similar shape to those found for flat samples of this material and shows a qualitative anticorrelation with the hardness depth profile. © *2009 American Institute of Physics*. [DOI: 10.1063/1.3106662]

I. INTRODUCTION

Photothermal radiometry is a well established tool for the thermophysical characterization and the nondestructive evaluation of a wide variety of materials. For decades, research in photothermal radiometry has been restricted to samples with flat surfaces.[1] However, in recent years, several thermal-wave studies of curvilinear (cylindrical and spherical) solids have been published,[2–8] where both solids with homogeneous thermophysical properties and multilayered materials have been analyzed. Those studies have been used to measure the thermal conductivity and/or diffusivity of homogeneous rods, tubes and balls, using modulated or pulsed photothermal radiometry. In a recent paper, the effective case depth of hardened steel rods with radii ranging from 1 to 10 mm has been obtained by fitting the frequency spectra of the amplitude and phase of the surface temperature to a two-layer model, i.e., an effective outer case hardened layer and an inner unhardened core.[9] This method is stable and simple, but only approximately valid since the hardened layer, which actually has a continuously varying thermal conductivity, has been modeled as a homogeneous layer with an effective (average) thermal conductivity. Actually, the discrepancies between the theoretical fits and the experiments, especially in the frequency range between 50–500 Hz, indicate that this method does not accurately recover the thermophysical property depth profiles of curvilinear materials from information embedded in the experimental thermal-wave frequency spectrum.

In this paper we calculate the thermal-wave field (ac temperature, or simply, temperature) of a multilayered cylinder, as well as that of a cylinder in which the radial thermal conductivity varies continuously. It is demonstrated numerically that the thermal-wave field from a cylindrical solid with a continuously variable radial thermal conductivity is well reproduced by using a multilayer approximation with a small number of layers, provided their thickness is not constant, but becomes thinner closer to the surface. Accordingly, the multilayered model with 20 layers has been used to fit the same experimental data as in Ref. 9 in order to reconstruct the entire thermal conductivity depth profile of hardened steel rods. The recovery of the radial dependence of the conductivity from measurements of the surface value of the thermal-wave field is a severely *ill-posed* nonlinear inverse problem, i.e., the unknown conductivity is extremely sensitive to errors and noise in the photothermal signal. In order to retrieve stable inversions there are two possibilities: the simpler one is to use very few unknowns (as was the case in Ref. 9) and the other one is to apply some kind of regularization method in the inversion.[10] In this paper we combine both; we applied Tikhonov regularization for the nonlinear inverse problem, using layers of different thicknesses to avoid a large number of unknowns.

The agreement between experimental data and theoretical fits is very good in the whole frequency range of the experiments (0.5 Hz to 10 kHz). The reconstructed radial thermal conductivity depth profile has a similar shape to those found for flat samples. Moreover, there is qualitative anticorrelation with the hardness depth profile, which has been obtained from mechanical indentation tests. This work provides the mathematical tools for applying photothermal

a)Electronic mail: agustin.salazar@ehu.es.

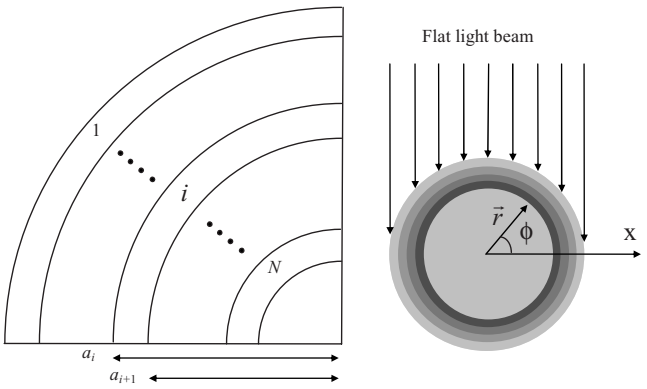

FIG. 1. (a) Cross-section of a multilayered cylinder made of N layers. (b) Scheme of the illumination and the coordinates used in the theory.

radiometry to retrieve the hardness case depth profile of nails, tubes, and other metallic pieces of cylindrical shape in a nondestructive way.

II. THEORY

In this section we first calculate the surface temperature of an infinitely long and opaque cylinder illuminated by a modulated light beam. In Sec. II A, we deal with a multilayered cylinder. Next, we address the problem of a solid cylinder, the radial thermal conductivity of which varies continuously with depth as a polynomial.

A. Multilayered cylinder

Let us consider an infinite and opaque multilayered cylinder, which is illuminated by a uniform light beam of intensity I_o modulated at a frequency f ($\omega=2\pi f$). It is made of N layers of different thicknesses and thermal properties. The properties of layer i are labeled by subindex i and its outer and inner radii by a_i and a_{i+1}, respectively (see Fig. 1). By using the thermal quadrupole method[11] the temperature oscillation at the outer surface of the cylinder is given by[5]

$$T(a_1,\phi)=\frac{I_o}{2}\sum_{m=-\infty}^{\infty}\frac{|\cos(m\pi/2)|}{\pi(1-m^2)}\frac{A'_m}{C'_m+A'_m h}e^{im\phi}, \tag{1}$$

where h is the heat transfer coefficient at the cylinder surface, which accounts for heat losses due to convective and radiative heat transfer. The frequency dependent coefficients A'_m and C'_m are obtained from the following matrix product:

$$\begin{pmatrix}A'_m\\C'_m\end{pmatrix}=\left[\prod_{i=1}^{N}\begin{pmatrix}A_{mi}&B_{mi}\\C_{mi}&D_{mi}\end{pmatrix}\right]\times\begin{pmatrix}J_{m,N+1}(q_{N+1}a_{N+1})\\K_{N+1}q_{N+1}J'_{m,N+1}(q_{N+1}a_{N+1})\end{pmatrix},\quad m=-\infty,\ldots,0,\ldots,+\infty \tag{2}$$

with

$$A_{mi}=[H'_{mi}(q_i a_{i+1})J_{mi}(q_i a_i)-J'_{mi}(q_i a_{i+1})H_{mi}(q_i a_i)]E_{mi},$$

$$B_{mi}=[J_{mi}(q_i a_{i+1})H_{mi}(q_i a_i)-H_{mi}(q_i a_{i+1})J_{mi}(q_i a_i)]/E_{mi}K_i q_i,$$

$$C_{mi}=K_i q_i[H'_{mi}(q_i a_{i+1})J'_{mi}(q_i a_i)-J'_{mi}(q_i a_{i+1})H'_{mi}(q_i a_i)]/E_{mi},$$

$$D_{mi}=[J_{mi}(q_i a_{i+1})H'_{mi}(q_i a_i)-H_{mi}(q_i a_{i+1})J'_{mi}(q_i a_i)]/E_{mi}$$

and

$$E_{mi}=H'_{mi}(q_i a_{i+1})J_{mi}(q_i a_{i+1})-H_{mi}(q_i a_{i+1})J'_{mi}(q_i a_{i+1}).$$

Here $q=\sqrt{i\omega/D}$ is the thermal wave vector, K is the thermal conductivity, D is the thermal diffusivity, and J_m, H_m, J'_{mi} and H'_{mi} are the Bessel and Hankel functions of the first kind of the mth order and their derivatives.

B. Continuously varying thermal conductivity

Now we consider an opaque bulk cylinder of radius a_1 whose thermal conductivity varies radially as a polynomial: $K(r)=K_o+K_1 r+K_2 r^2+\ldots..+K_p r^p$, while its heat capacity $\rho c=K/D$ remains constant. This condition applies for some hardened steels and has been confirmed experimentally.[12] The cylinder is illuminated by light of homogeneous spatial distribution as shown in Fig. 1. We look for solutions to the heat conduction equation representing incoming thermal waves: $\theta(\vec{r},t)=T(\vec{r})e^{-i\omega t}$. The spatial component of the thermal-wave field satisfies the following equation:

$$\vec{\nabla}(K\vec{\nabla}T)+i\omega\rho cT=0 \tag{3}$$

that in cylindrical coordinates can be written as

$$K\frac{\partial^2 T}{\partial r^2}+\left(\frac{K}{r}+\frac{dK}{dr}\right)\frac{\partial T}{\partial r}+\frac{K}{r^2}\frac{\partial^2 T}{\partial\phi^2}+i\omega\rho cT=0. \tag{4}$$

Using separation of variables we look for solutions of the form

$$T(r,\phi)=\sum_{m=-\infty}^{\infty}G_m R(r)e^{im\phi}=\sum_{m=-\infty}^{\infty}G_m\left(\sum_{n=0}^{\infty}d_n r^{n+|m|}\right)e^{im\phi}, \tag{5}$$

which represent the ingoing thermal wave. The radial function $R(r)$ in Eq. (5) satisfies the ordinary differential equation

$$\frac{d^2R}{dr^2}+\left(\frac{1}{r}+\frac{1}{K}\frac{dK}{dr}\right)\frac{dR}{dr}+\left(\frac{i\omega\rho c}{K}-\frac{m^2}{r^2}\right)R=0. \tag{6}$$

By substituting Eq. (5) into Eq. (4) the coefficients d_n are obtained. They satisfy the following recurrence relation:

$$\begin{aligned}d_{n+2}[(n+2)(n+2)+|m|(2n+4)]K_o+d_{n+1}[(n+2)(n+1)+|m|(2n+3)]K_1+d_n[(n+2)n+|m|(2n+2)]K_2+d_{n-1}[(n+2)(n-1)+|m|(2n+1)]K_3\\+\ldots\ldots.+d_{n-p+2}[(n+2)(n-p+2)+|m|(2n-p+4)]K_p+i\omega\rho cd_n=0\end{aligned} \tag{7}$$

with $d_o=1$. This recurrence relation follows for $n\geq p-2$, where p is the order of the polynomial. For instance, the first

two coefficients are $d_1=-K_1/K_o|m|/1+2|m|$ and $d_2=-d_1K_1/K_o(2+3|m|/4+4|m|)-K_2 2|m|+i\omega\rho c/K_o(4+4|m|)$. The coefficients G_m in Eq. (5) are obtained from the heat flux continuity on the cylindrical surface

$$K(r=a_1)\left.\frac{dT}{dr}\right|_{r=a_1}=\frac{I_o}{2}\sum_{m=-\infty}^{\infty}\frac{|\cos(m\pi/2)|}{\pi(1-m^2)}e^{im\phi}-hT(a_1), \tag{8}$$

where the summation term on the right-hand side represents the Fourier decomposition of the incident light flux, $(I_o \sin\phi)/2$ for $0\leq\phi\leq\pi$ and zero for all other angles [see Fig. 1(b)]. The second term accounts for surface heat losses.

Substitution of Eq. (5) into Eq. (8) and solution for the coefficients G_m yield the thermal-wave field at any point in the solid cylinder,

$$T(r,\phi)=\frac{I_o}{2}\sum_{m=-\infty}^{\infty}\frac{|\cos(m\pi/2)|}{\pi(1-m^2)}\frac{R(r)}{K(a_1)R'(a_1)-hR(a_1)}e^{im\phi}, \tag{9}$$

where $R'(r)$ is the derivative of $R(r)$, as it is defined in Eq. (5).

It is worth noting that Eq. (9) allows the calculation of the thermal-wave field at any point inside the cylinder, while Eq. (1) is only valid for the surface value of the field of a multilayered cylinder. This is actually the main limitation of the quadrupole method. However, Eq. (1) has the advantage of being more stable for the inverse problem and it will be used in this work to reconstruct the radial thermal conductivity profile of hardened steel rods. In Sec. III we will verify numerically that the surface temperature obtained for a multilayered cylinder, Eq. (1), converges to the exact solution given by Eq. (9), as the number of layers increases. Moreover, it will be demonstrated that complete convergence can be attained by using only a small number of layers. This result yields theoretical support for using Eq. (1) for the inverse problem.

III. NUMERICAL CALCULATIONS

In what follows all simulations are performed for AISI 1018 carbon steel rods, whose thermal properties are[13] $K=51.9$ $\mathrm{Wm^{-1}\,K^{-1}}$, $D=13.6$ $\mathrm{mm^2/s}$, and $\rho c=K/D=3.82\times10^6$ $\mathrm{Jm^{-3}\,K^{-1}}$. Due to the hardening process (carburizing and quenching) the thermal conductivity is highly reduced at the sample surface, while it remains unchanged at the center of the cylindrical sample. In between, the thermal conductivity decreases monotonically following a radial dependence curve, the reconstruction of which is the problem at hand.

In Fig. 2 we show the frequency dependence of the amplitude and phase of the surface thermal-wave field of a 1 mm radius cylinder, the thermal conductivity of which varies according to the equation $K(r)=(51.9-51.9/2\times10^9\ r^3)$ $\mathrm{Wm^{-1}\,K^{-1}}$, while the heat capacity $\rho c=3.82\times10^6$ $\mathrm{Jm^{-3}\,K^{-1}}$ remains constant. The number of terms that must be used to guarantee the convergence of Eq. (9) depends on the radius and thermal properties of the cylinder. We have performed several tests varying such properties

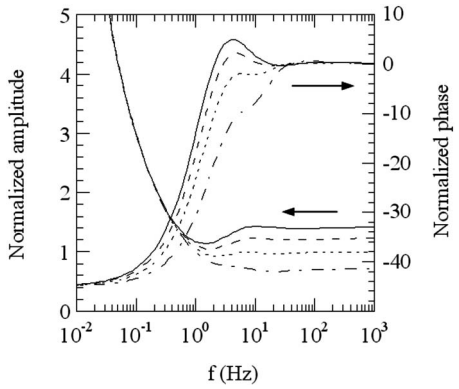

FIG. 2. Frequency dependence of the normalized amplitude and phase of the surface temperature of a rod of radius 1 mm whose thermal conductivity varies according to $K(r)=(51.9-51.9/2\times10^9\ r^3)$ $\mathrm{Wm^{-1}\,K^{-1}}$, while $\rho c=3.82\times10^6$ $\mathrm{Jm^{-3}\,K^{-1}}$ is kept constant. Four surface positions are calculated: $\phi=\pi/2$ (continuous line), $\phi=\pi/3$ (dashed line), $\phi=\pi/4$ (dotted line), and $\phi=\pi/6$ (dashed-dotted line).

over a wide range of values and we have concluded that the convergence is assured by using $m=100$ and $n=60$. In all simulations the cylindrical thermal-wave field is normalized to an infinitely thick flat slab of unhardened AISI 1018 steel. Calculations are performed at various angles: $\phi=\pi/2$ (the north pole of the cylinder), $\pi/3$, $\pi/4$, and $\pi/6$. As can be seen, at high frequencies the normalized phase goes to zero, while the normalized amplitude converges to a constant value. This can be understood since at high frequencies both rod and slab are thermally thick, and their respective surface temperature are

$$T_{\mathrm{rod}}(\phi)\approx\frac{I_o}{2}\sin\phi\frac{e^{-i\pi/4}}{e_s\sqrt{\omega}}, \tag{10a}$$

$$T_{\mathrm{slab}}\approx\frac{I_o}{2}\frac{e^{-i\pi/4}}{e_o\sqrt{\omega}}, \tag{10b}$$

where $e=\sqrt{\rho cK}$ is the thermal effusivity and subscripts o and s stand for the unhardened value and the surface value, respectively. Accordingly, the normalized temperature, $T_n(\phi)\approx(e_o/e_s)\sin\phi$, has a frequency independent amplitude and a null phase. In our example of Fig. 2, for $\phi=\pi/2$, $\pi/3$, $\pi/4$, and $\pi/6$, the normalized temperature is $T_n=1.414$, 1.225, 1.00, and 0.707, respectively. On the other hand, at very low frequencies the rod is thermally thin (i.e., high amplitude and phase equal to $-90°$), while the infinitely thick slab remains thermally thick (i.e., low amplitude and phase equal to $-45°$). Therefore, the normalized amplitude goes to infinity and the normalized phase goes to $-45°$, as can be seen in Fig. 2.

Now we want to reproduce the surface thermal-wave field corresponding to a cylinder with a continuously varying thermal conductivity, as obtained from Eq. (9), by means of a multilayered cylinder made of a discrete number of layers, using Eq. (1). In fact, we are interested in estimating how many layers are needed to obtain the exact thermal-wave field frequency spectrum corresponding to a continuous $K(r)$ depth profile. In Fig. 3 we show the thickness and thermal conductivity of a six-layer cylinder that roughly matches the

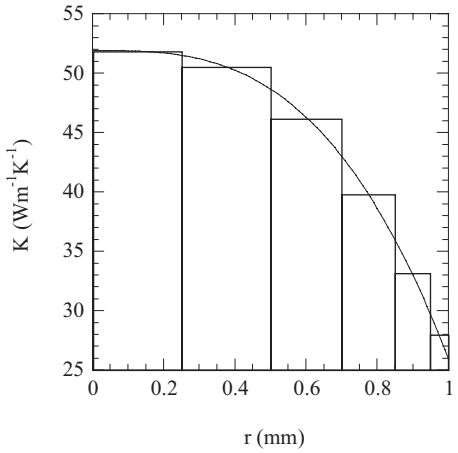

FIG. 3. Simulation of a 1 mm radius rod with continuously varying thermal conductivity by using six layers rod of the same radius. The height of each layer indicates its thermal conductivity, which is taken to be the thermal conductivity at the center of the layer.

continuous thermal conductivity profile used in Fig. 2. As can be seen, we have used layers of different thicknesses, thinner near the surface and thicker near the center of the cylinder. In particular, inner layer thicknesses are multiples of that of the outer shell. Note that the origin of the cylindrical coordinate system is located at the center of the cylinder, as shown in Fig. 1(b). This thickness adaptive layering procedure is supported by the fact that the surface value of the thermal-wave field is more sensitive to what happens close to the surface. The question is to find the minimum number of layers that reproduces the closest approximation to the thermal-wave field value as calculated from Eq. (9). In Fig. 4 we show the frequency dependence of the normalized amplitude and phase of the surface temperature at the north pole ($\phi=\pi/2$) of a rod of radius 1 mm. The continuous line represents the calculation performed using Eq. (9) with the same parameters as in Fig. 2. The dotted line corresponds to the calculation of Eq. (1) for a three-layer cylinder, the dashed line for a six-layer cylinder, and the dashed-dotted line for a ten-layer cylinder. As can be seen, the results differ at high

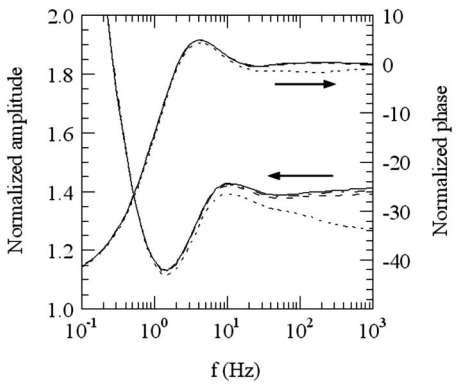

FIG. 4. Frequency dependence of the normalized amplitude and phase of the surface temperature at the north pole ($\phi=\pi/2$) of a 1 mm radius rod. The continuous line is the calculation performed using Eq. (9) with the same parameters as in Fig. 3. The dotted line corresponds to the calculation of Eq. (1) for a three-layer cylinder, the dashed line for a six-layer cylinder, and the dashed-dotted line for a ten-layer cylinder.

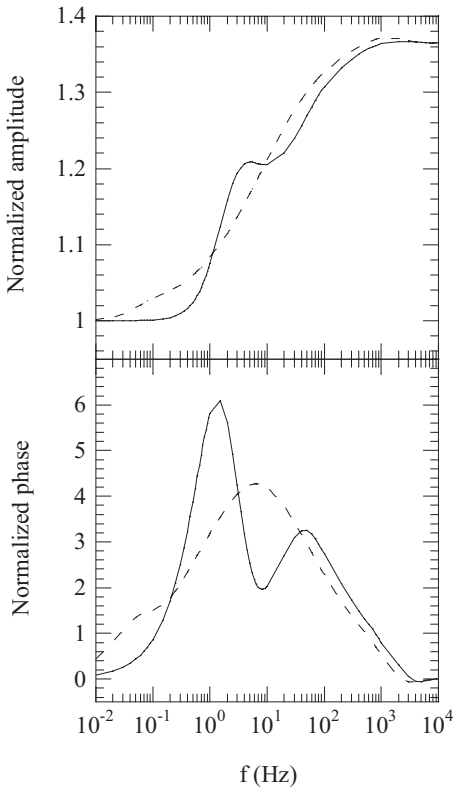

FIG. 5. Effect of the radial shape on the surface temperature. The continuous line corresponds to the frequency dependence of the normalized amplitude and phase at the north pole ($\phi=\pi/2$) of a 1 mm radius rod made of six layers whose thermal conductivity varies as shown in Fig. 3. The dashed line stands for a flat sample whose first millimeter is made of six layers with a variable thermal conductivity according to Fig. 3.

frequencies, but using ten layers the temperature is accurately reproduced for this rather smooth conductivity depth profile.

In Fig. 5 we show the comparison between the frequency dependence of the temperature corresponding to a 1 mm radius rod (continuous line) and to a flat sample (dashed line). Calculations have been performed at the north pole ($\phi=\pi/2$) of a 1 mm radius rod made of six layers whose thermal conductivity varies as shown in Fig. 3, and at the front surface of a flat sample whose first millimeter is made up of six layers with a thermal conductivity varying according to Fig. 3. The frequency scan corresponding to the inhomogeneous rod is normalized with respect to a homogeneous rod of the same radius and constant thermal conductivity ($K=51.9$ Wm^{-1} K^{-1}), while the temperature of the inhomogeneous flat sample is normalized with respect to a homogeneous flat sample ($K=51.9$ Wm^{-1} K^{-1}). Although both results coincide at very low and very high frequencies, the intermediate behavior (where experimental data are obtained) is very different and justifies the need of using the cylindrical model introduced in Sec. II, since the approximation of the rod by a planar model does not hold.

IV. INVERSION PROCEDURE AND DISCUSSION

In order to reconstruct the thermal conductivity profile of hardened steel rods we have used the experimental data of Ref. 9, where hardened C1018 steel rods of several diameters

were measured using a photothermal radiometry system. However, in that reference the experimental data were fitted using a two-layer model, i.e., an outer hardened layer with constant thermal properties and an inner layer of unhardened steel. In this manner the authors were able to estimate the effective thickness of the hardened layer, which is valuable information for many industrial applications. Actually, the quality of the fits (see Figs. 4 and 9 in Ref. 9) is quite good, bearing in mind the simplicity of the model. That agreement is due to the fact that to fit the experimental data to a two-layer rod, both the thermal conductivity and the thermal diffusivity of the hardened layer were taken as free parameters. The assumption, however, results in variable heat capacity $\rho c = K/D$, which should remain constant during the case hardening process in some steels.[12] Moreover, there are some discrepancies between the experimental points and the theoretical fits, especially at intermediate frequencies (50–500 Hz), which are explained by the fact that the thermal properties of the hardened layer are not constant, but there is a gradual change from the hardened surface to the unhardened core.

Generally speaking, ill-posed inverse problems can be solved either as a parameter estimation or as a function estimation approach. (a) If some information is available on the functional form of the unknown quantity, the inverse problem can be reduced to the estimation of a finite number of unknown parameters (chosen in advance). This approach is stable and does not need any additional regularization since the limited number of unknowns acts as regularization. (b) If no prior information is available on the functional form of the unknown, the inverse problem can be regarded as a functional estimation approach in an infinite dimensional space of functions. In their numerical approximation, the number of unknowns should remain large and could not be used as the main regularization parameter, being necessary to use additional regularizations. In this paper we have chosen the function estimation approach for the inversion, since we only use prior information about the range of values of the conductivity, but we do not use any hypothesis about their functional form. In this context of a reasonably large number of unknowns, we opt for a multilayered model instead of a polynomial representation of the conductivity because the monomial basis of polynomials includes additional instabilities when it comes to the inversion.

In order to reflect the actual inhomogeneous structure in hardened steels and improve the quality of the fits we have used the multilayered model introduced in Sec. II to fit the same experimental data, keeping constant $\rho c = 3.82 \times 10^6$ $\mathrm{Jm^{-3}\,K^{-1}}$ over all the layers. According to the multilayered structure shown in Fig. 1, we assume that the conductivity $K(r)$ is a piecewise constant function, with N layers of constant conductivities K_i as the unknowns. To extract information about the thermal conductivity profile of the hardened rods from the experimental temperature T_{exp} we have used a nonlinear least-squares fitting of the experimental data using the residual function (g), which is usually defined as

$$g(K_1, \ldots, K_N, \varphi) = \sum_{j=1}^{M} |T_{\mathrm{th}}(K_1, \ldots, K_N, \varphi, f_j) - T_{\mathrm{exp}}(f_j)|^2, \tag{11}$$

where f_j are the experimental modulation frequencies, φ defines the polar coordinate of the measurement point with respect to the laser beam axis (see Fig. 3 in Ref. 9), and $T_{\mathrm{th}}(K_1, \ldots, K_N, \varphi, f_j)$ is the calculated thermal-wave field value obtained by means of Eq. (1) at frequency f_j. Both T_{exp} and T_{th} refer to the normalized temperatures with respect to an infinitely thick flat slab of unhardened AISI 1018 steel. The sum runs over all M frequencies of the experiment. However, the contribution of the high frequency range to g is very large, compared to the medium and low frequencies. This means that the highest frequencies of the experiment are very well fitted but the low frequency range is poorly fitted, a typical situation for diffusion-wave fields. For this reason, we have introduced a weighing factor[14] to reduce the contribution of the highest frequencies in Eq. (11),

$$g(K_1, \ldots, K_N, \varphi) = \sum_{j=1}^{M} \frac{1}{[1 + \ln(1 + f_j)]^2} |T_{\mathrm{th}}(K_1, \ldots, K_N, \varphi, f_j) - T_{\mathrm{exp}}(f_j)|^2. \tag{12}$$

Moreover, the presence of this factor softens the effect of the increasing experimental noise at high frequencies.

Unfortunately, due to the fact that this inverse problem is ill-posed and since errors either in the model or in the measurements cannot be avoided, a straightforward minimization of g in Eq. (12) leads to totally unrealistic thermal conductivity reconstructions. To stabilize the minimization we introduce a new term in g, which is the so-called Tikhonov penalty term,[10]

$$g(K_1, \ldots, K_N, \varphi) = \alpha \sum_{i=1}^{N} (K_i - K_i^0)^2 + \sum_{j=1}^{M} \frac{1}{[1 + \ln(1 + f_j)]^2} |T_{\mathrm{th}}(K_1, \ldots, K_N, \phi, f_j) - T_{\mathrm{exp}}(f_j)|^2, \tag{13}$$

where $\alpha > 0$ is a small regularization parameter and K_i^0 is an initial guess of the conductivity of the ith layer. In this initial guess we use prior information on the case hardening process taking a linear steplike conductivity depth profile with $K_1^0 = 20$ $\mathrm{Wm^{-1}\,K^{-1}}$ and $K_N^0 = 51.9$ $\mathrm{Wm^{-1}\,K^{-1}}$. It should be noted that although the penalty term stabilizes the minimization process, it also adds an additional error to the model. The key point is to choose a suitable value of α that guarantees stability with the lowest additional error.

In order to incorporate the Tikhonov penalty term we use a variant of the iterative Levenberg–Marquardt method suggested by Bakushinsky[15] to minimize the function g in Eq. (13). It is worth noting that the singular value decomposition approach could be used as an alternative regularization method, as was done for planar samples after linearization of the problem,[16–18] but it is more computer time consuming in

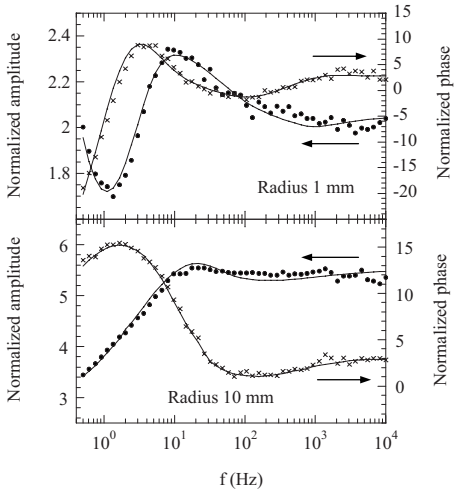

FIG. 6. Normalized amplitude (dots) and phase (crosses) of the photothermal radiometry measurements performed on two hardened steel rods whose radii are 1 and 10 mm. The continuous line is the best fit to Eq. (1) using 20 layers.

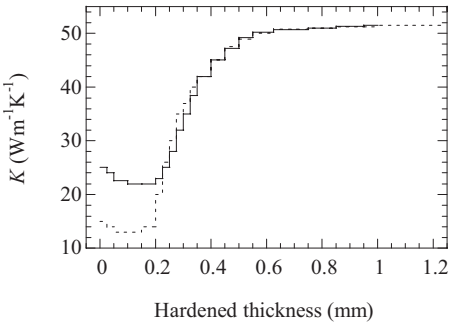

FIG. 7. Reconstructed depth profile of the thermal conductivity of the two rods of Fig. 5. Continuous line stands for the 1 mm radius rod and the dashed-line for the 10 mm radius rod.

our direct nonlinear approach. To avoid instabilities, iterations should stop at a point where α is not too small. We stop iterations when the second term in Eq. (13) is on the order of the experimental noise, according to the Morozov discrepancy principle.[19] If we allowed further iterations, we would obtain better fittings characterized by a smaller value of g, but leading to thermal conductivity depth profiles lacking any physical meaning.

As a consistency test we fitted the experimental data using only two layers, with freely variable thermal conductivity and diffusivity of the outer layer, and we obtained the same results as in Ref. 9, which are affected by an uncertainty of 2.5%. This uncertainty is due to combined uncertainties of the experimental data and the simplicity of the model. Then, we used a ten-layer model with freely variable thermal conductivity but constant ρc to simulate the hardened region. In the first fittings, we used layers of increasing thickness as they are deeply buried inside the cylinder. As the reconstructed thermal conductivity profile showed an almost flat behavior close to the surface followed by a steep slope in the middle region, we increased the total number of layers up to 20 and made them thinner around the steep region. The dots in Fig. 6 are the experimental data of the frequency dependence of the normalized amplitude and phase of the surface IR signal corresponding to two hardened C1018 steel rods of radii 1 and 10 mm. The continuous lines correspond to our best fit obtained with 20 layers. The fitted φ values are 4° and 43° for the rods of radii 1 and 10 mm, respectively, which are very close to those obtained in Ref. 9. It is worth noting that the uncertainty in the value of φ has small influence in the fitting curve provided that the angle is small enough ($\varphi < 45°$). For instance, an error $\Delta\varphi = 2°$ produces an immeasurable change in the fitting curve for $0° < \varphi < 10°$, while this change increases to 1% for $40° < \varphi < 45°$. Only at high angles, $\varphi > 60°$, the accuracy in the experimental φ value is critical for the accuracy of the fitting curve. As expected, the fits are better than those obtained with only two layers and correspond to a smaller uncertainty of 1.5%. In this case, the uncertainty of the fit is mainly the result of noise in the experimental data. However, although the accuracy gain of using 20 instead of two layers seems to be small, it has been obtained by keeping ρc constant, which is more realistic as stated before. Actually, the experimental results can hardly be fitted if only two layers with constant ρc are used. In fact, the fits of Ref. 9 were obtained with a hardened layer with a heat capacity that changes from 3.82×10^6 $\mathrm{Jm^{-3}\,K^{-1}}$ for the unhardened steel to 2.24×10^6 $\mathrm{Jm^{-3}\,K^{-1}}$ or the 1 mm radius rod or to 1.89×10^6 $\mathrm{Jm^{-3}\,K^{-1}}$ for the rod of radius 10 mm, which represents a 50% variation in self-consistency.[20]

Paoloni *et al.*[21] analyzed the effect of the lateral heat diffusion due to the nonuniform shape of the laser beam on the reconstructed depth profile of hardened steel plates. That effect was mainly due to the use of a laser beam of Gaussian profile, while the experimental results used in this work are obtained with a diode laser with a flat profile. Therefore lateral heat diffusion has been neglected in this study.

Figure 7 shows the reconstructed thermal conductivity profiles corresponding to the fits of Fig. 6. Note that in order to represent the reconstructed $K(r)$ of the two steel rods in the same figure we have taken the origin of r at the cylinder surface. Their shapes are very similar to those found in flat surface geometries,[22–26] and they are in good qualitative anticorrelation with the hardness depth profile obtained by mechanical indentation testing performed on these rods (see Fig. 6 in Ref. 9), although the depth penetration of K (about 0.6 mm) is smaller than the nominal hardness case depth of 1 mm. It is worth mentioning that although the penetration depth is similar for both rods, the near surface value of the thermal conductivity is not the same in both cases. The reconstructed $K(r)$ curve near the surface exhibits a ~0.2 mm layer with $\mathrm{K} \sim 15$ W/mK for the 10 mm radius steel rod and $\mathrm{K} \sim 22$ W/mK for the 1 mm radius rod. A possible explanation of this discrepancy is that, for the thicker rod, much lower frequencies should be used in order to reconstruct the entire depth range of the thermal conductivity. According to Fig. 4, both the amplitude and the phase show a maximum and a minimum, provided a very wide frequency range is scanned. However, for the 10 mm radius rod, only the maximum of the amplitude and the shallow minimum of the phase have been included in the frequency responses. Lower frequencies would be required in order to include the remain-

ing extrema, which are included in the 1 mm cylinder frequency response. Therefore, we conclude that the most reliable $K(r)$ reconstruction corresponds to the 1 mm radius rod.

V. CONCLUSIONS

In summary, the thermal quadrupole method was used to calculate the surface temperature of an opaque multilayered cylinder when it is illuminated by a modulated uniform light beam. Furthermore, we also calculated the surface temperature of a solid cylinder with a radial thermal conductivity depth profile when it is illuminated under the same modulated conditions. It was also demonstrated numerically that the ac temperature field of a cylindrical solid with a continuously variable radial thermal conductivity is well reproduced by using a multilayer approximation with a rather small number of layers, provided their thickness is not constant, but becomes thinner closer to the surface. According to this result, and taking into account that the inversion procedure is more stable for the multilayered than for the continuous model, we have applied an inverse procedure based on the multilayered cylinder to reconstruct the radial thermal conductivity profile of hardened C1018 steel rods. It is shown that it exhibits an anticorrelation with hardness depth profile, in agreement with earlier studies. As a final conclusion, it is claimed that the mathematical tools given in this paper allow for photothermal radiometric nondestructive characterization of the thermophysical properties of hardened steel wires, tubes and nails, in which the thermal conductivity varies radially depending on the type of the applied thermal treatment.

ACKNOWLEDGMENTS

This work has been supported by the Ministerio de Educación y Ciencia through Research Grant No. MAT2005-02999, by the Universidad del País Vasco through Research Grant No. DIPE06/06 and by the Diputación General de Aragón. C. Wang would thank the financial support from the National Natural Science Foundation of China (Grant No. 60877063) and Scientific Research Foundation for Returned Scholars, Ministry of Education of China. A. Mandelis is grateful for the support of the Natural Sciences and Engineering Research Council of Canada.

[1] D. P. Almond and P. M. Patel, *Photothermal Science and Techniques* (Chapman and Hall, London, 1996).
[2] C. Wang, A. Mandelis, and Y. Liu, J. Appl. Phys. **96**, 3756 (2004).
[3] C. Wang, A. Mandelis, and Y. Liu, J. Appl. Phys. **97**, 014911 (2005).
[4] A. Salazar, F. Garrido, and R. Celorrio, J. Appl. Phys. **99**, 066116 (2006).
[5] A. Salazar and R. Celorrio, J. Appl. Phys. **100**, 113535 (2006).
[6] C. Wang, Y. Liu, A. Mandelis, and J. Shen, J. Appl. Phys. **101**, 083503 (2007).
[7] N. Madariaga and A. Salazar, Appl. Phys. (Berl.) **101**, 103534 (2007).
[8] E. Apiñaniz, A. Mendioroz, N. Madariaga, A. Oleaga, R. Celorrio, and A. Salazar, J. Phys. D **41**, 015403 (2008).
[9] C. Wang and A. Mandelis, Rev. Sci. Instrum. **78**, 054902 (2007).
[10] H. W. Engl, M. Hanke, and A. Neubauer, *Regularization of Inverse Problems* (Kluwer Academic Publisher, Dordrecht, 2000).
[11] D. Maillet, S. André, J. C. Batsale, A. Degiovanni, and C. Moyne, *Thermal Quadrupoles* (Wiley, New York, 2000).
[12] H. G. Walther, D. Fournier, J. C. Krapez, M. Luukkala, B. Schmitz, C. Sibilia, H. Stamm, and J. Thoen, Anal. Sci. **17**, s165 (2001).
[13] *Metals Handbook*, 10th ed. (ASM International, Materials Park, OH, 1990), Vol. 1, p. 196.
[14] M. N. Özisik and H. R. B. Orlande, *Inverse Heat Transfer: Fundamentals and Applications* (Taylor & Francis, New York, 2000), p. 14.
[15] A. B. Bakushinsky, Comput. Math. Math. Phys. **32**, 1353 (1992).
[16] M. Bertolotti, R. Li Voti, G. L. Liakhou, and S. Paoloni, and C. Sibilia, AIP Conf. Proc. **463**, 24 1998.
[17] C. Glorieux, R. Li Voti, J. Thoen, M. Bertolotti, and C. Sibilia, Inverse Probl. **15**, 1149 (1999).
[18] J. F. Power, Rev. Sci. Instrum. **73**, 4057 (2002).
[19] T. Bonesky, Inverse Probl. **25**, 015015 (2009).
[20] The heat capacity values in condensed matter are always in the range from 1.0×10^6 to 4.0×10^6 Jm^{-3} K^{-1} [A. Salazar, Eur. J. Phys. **24**, 351 (2003)]. For this reason a reduction of 50% is considered large.
[21] S. Paoloni, P. Mayr, C. Glorieux, R. Li Voti, H. Bentefour, and J. Thoen, Anal. Sci. **17**, s406 (2001).
[22] M. Munidasa, F. Funak, and A. Mandelis, J. Appl. Phys. **83**, 3495 (1998).
[23] R. Kolarov and T. Velinov, J. Appl. Phys. **83**, 1878 (1998).
[24] Y. Z. Zhao, S. Y. Zhang, J. C. Cheng, Y. K. Zhang, and W. H. Xu, Appl. Phys. A: Mater. Sci. Process. **A71**, 319 (2000).
[25] L. Nicolaides, A. Mandelis, and C. J. Beingessner, J. Appl. Phys. **89**, 7879 (2001).
[26] D. Kruse, H. Prekel, G. Goch, and H. G. Walther, Proc. Est. Acad. Sci., Phys., Math. **13**, 423 (2007).